

RESEARCH

Open Access



Investigation of geomechanical properties of tephra relevant to roof loading for application in vulnerability analyses

Sara Osman^{1*}, Mark Thomas¹, Julia Crummy² and Stephen Carver³

Abstract

Tephra fall can lead to significant additional loading on roofs. Understanding the relevant geomechanical properties of tephra is critical when assessing the vulnerability of buildings to tephra fall and designing buildings to withstand tephra loads. Through analysis of published data and new experimental results on dry tephra (both natural samples from Ascension Island, South Atlantic and synthetic tephra made from crushed aggregates), we discuss the geomechanical properties of tephra relevant to roof loading, which include bulk density, grain size distribution and internal angle of friction. Compiled published data for deposits from 64 global eruptions reveal no clear trend in deposit densities based on magma composition or eruption size. The global data show a wide range of values within single eruptions and between eruptions of similar compositions. Published grain size distributions near to source (≤ 10 km) vary widely but again there are no clear trends relating to magma composition. We used laboratory tests to investigate the internal angle of friction, which influences deposit sliding behaviour. For dry tephra, at the low normal stresses likely to be experienced in roof loads (≤ 35 kPa), we found similar values across all our tests ($35.8^\circ - 36.5^\circ$) suggesting that any internal sliding will be consistent across a variety of deposits. By considering different magma compositions, densities and grain size distributions, we have provided an envelope of values for deposit parameters relevant to roof loading, in which future eruptions are likely to sit. Finally, we created synthetic tephra (fine- and coarse-grained pumice and scoria) by crushing volcanic aggregates and compared it to samples from Ascension and published data. Our results reveal that synthetic tephra successfully replicated the properties relevant to loading, potentially reducing the need to collect and transport natural samples.

Keywords: Tephra fall, Roof loading, Building vulnerability, Friction angle, Bulk density, Grain size distribution

Introduction

During an explosive volcanic eruption, the fall out of tephra (ejected particles of all sizes) from the eruptive plume can lead to significant additional loading on roofs. Buildings close to an eruptive vent can sustain substantial damage or even collapse (e.g. Blong 2003; Jenkins et al. 2014; Hayes et al. 2019). Most recently, roof collapses

occurred following the April 2021 eruption of La Soufrière on St Vincent (Lesser Antilles).

The key factors that are thought to influence the load transferred to the roof by a tephra deposit, are magma composition and vesicularity, the size distribution and shape of the grains, and properties of the roof (Fig. 1). Magma properties influence the density of individual grains, while their size distribution and shape influence packing (Estrada 2016; Landauer et al. 2020). Deposit density depends on both grain

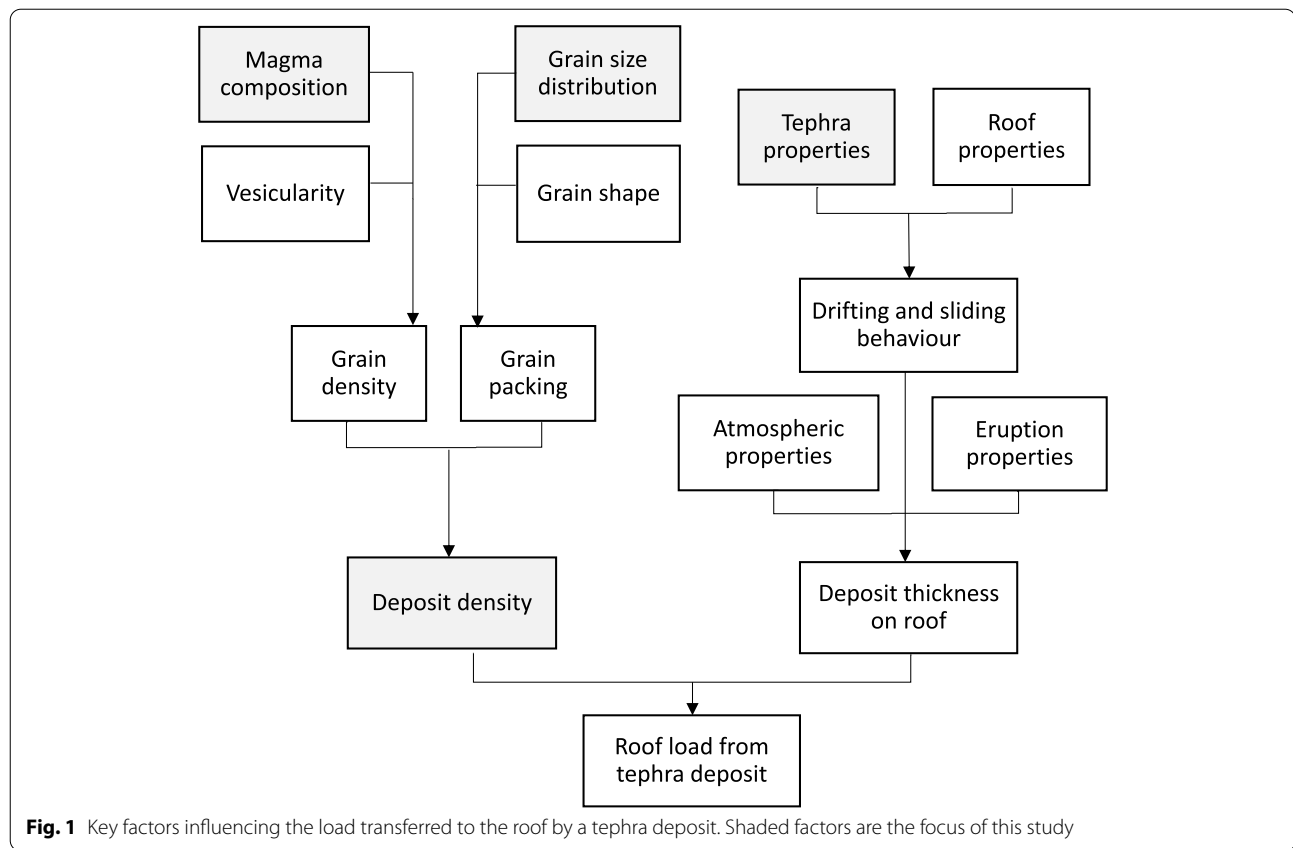
*Correspondence: eesjo@leeds.ac.uk

¹ University of Leeds, School of Earth and Environment, Woodhouse, Leeds LS2 9JT, UK

Full list of author information is available at the end of the article



© The Author(s) 2022. **Open Access** This article is licensed under a Creative Commons Attribution 4.0 International License, which permits use, sharing, adaptation, distribution and reproduction in any medium or format, as long as you give appropriate credit to the original author(s) and the source, provide a link to the Creative Commons licence, and indicate if changes were made. The images or other third party material in this article are included in the article's Creative Commons licence, unless indicated otherwise in a credit line to the material. If material is not included in the article's Creative Commons licence and your intended use is not permitted by statutory regulation or exceeds the permitted use, you will need to obtain permission directly from the copyright holder. To view a copy of this licence, visit <http://creativecommons.org/licenses/by/4.0/>. The Creative Commons Public Domain Dedication waiver (<http://creativecommons.org/publicdomain/zero/1.0/>) applies to the data made available in this article, unless otherwise stated in a credit line to the data.



density and packing and can also increase substantially if the deposit is wet (e.g. Blong 1981; Macedonio and Costa 2012; Hayes et al. 2019; Williams et al. 2021). The size and intensity of the eruption impact the height of the volcanic plume (e.g. Bonadonna and Costa 2013; Suzuki et al. 2016; Cassidy et al. 2018) and atmospheric processes, including wind velocity and precipitation, influence the transport and deposition of particles (e.g. Petersen et al. 2012; Bonadonna et al. 2015; Poulidis et al. 2018). In turn, these factors affect the amount of tephra deposited at any location. The load on the roof depends on the bulk density and thickness of the deposit, but tephra thickness can be altered after deposition by drifting and sliding. These processes are influenced by tephra properties, such as the internal angle of friction and grain size distribution, as well as the material, shape and pitch of the roof and the coefficient of friction between the tephra and the roof (e.g. Hampton et al. 2015).

The aim of this study is to discuss and present the geomechanical properties of tephra relevant to roof loading. Understanding these properties is critical

when assessing the vulnerability of buildings in areas at risk of tephra fall as they influence the additional load that is transferred to a roof and hence its likelihood of collapse. Estimating this additional loading is also important for building design, where building codes use a combination of historic records and experimental results to assess loads likely to occur within a building's lifespan. Snow loading, which is fundamentally similar to loading from tephra in that it is a granular air-fall deposit, is well characterised and routinely included in international design standards (e.g. British Standards Institution 2009; International Standards Organization 2013; American Society of Civil Engineers and Structural Engineering Institute 2017), but tephra fall is not routinely taken into account, and at the time of writing is not specifically considered in any international design standards or building codes.

This study forms part of a wider body of research investigating the potential of roof collapse by tephra loading with relevance to Ascension Island and the development of standards to account for tephra loads in building design. Ascension is a volcanically active UK Overseas

Territory in the south Atlantic with an area of 98 km² and ~780 residents. Because of Ascension's remote location and exposure to potential volcanic hazards, buildings could be vulnerable to collapse from any future explosive activity. In addition, Ascension tephra deposits vary widely in grain size and composition (e.g. Winstanley 2020; Preece et al. 2021), making it an ideal location to investigate any variation in the geomechanical properties of tephra, and whether synthetic tephra can be used in lieu of natural material.

In order to undertake the required laboratory tests, large volumes of tephra are required and these are not always easily obtained from natural sources due to the hazards associated with near-source sampling following an eruption and the costs of transporting large volumes of samples. We therefore investigated whether synthetic tephra (of unknown composition, made from crushing and sieving commercially available volcanic aggregates) could be used to model the properties of naturally occurring deposits that are relevant when considering roof loads (bulk density, grain size distribution and internal angle of friction). By comparing synthetic tephra of a non-specific composition to published data and the results from tests conducted as part of this study on Ascension tephra, the possibility of using commercially available aggregate to generate the volumes of material required for large scale testing can be assessed.

We compiled published density and grain size data for deposits from 64 global eruptions, measured the grain size distributions (GSDs) of samples of pumice, scoria and ash from Ascension and selected representative GSDs for our synthetic samples. We then used shear box tests to measure the internal angle of

friction of dry samples of both natural and synthetic material. The tests undertaken in this study were only performed on dry tephra and do not consider the saturated state of the deposit. Results for our synthetic samples matched well with both Ascension samples and published data from a wide range of eruptions; we can therefore be confident in using synthetic tephra to investigate the properties that control loading and sliding.

Methods

To ensure our test samples were representative of natural deposits, we compared them to published GSDs from global mafic, intermediate and silicic eruptions (listed in Table 1), focusing on proximal samples (≤ 10 km from source) to enable comparison with GSDs of samples from Ascension. The Ascension samples were sieved to 4 ϕ_g (63 μ m) diameter, with smaller particles analysed by dynamic image analysis (British Standards Institution 2006) using a Microtrac CAMSIZER[®] X2. These samples comprised trachytic ash, lithic-rich and lithic-poor trachytic pumice (Preece et al. 2021) and coarse-grained and fine-grained basaltic scoria (Winstanley 2020) from five locations shown in Fig. 2.

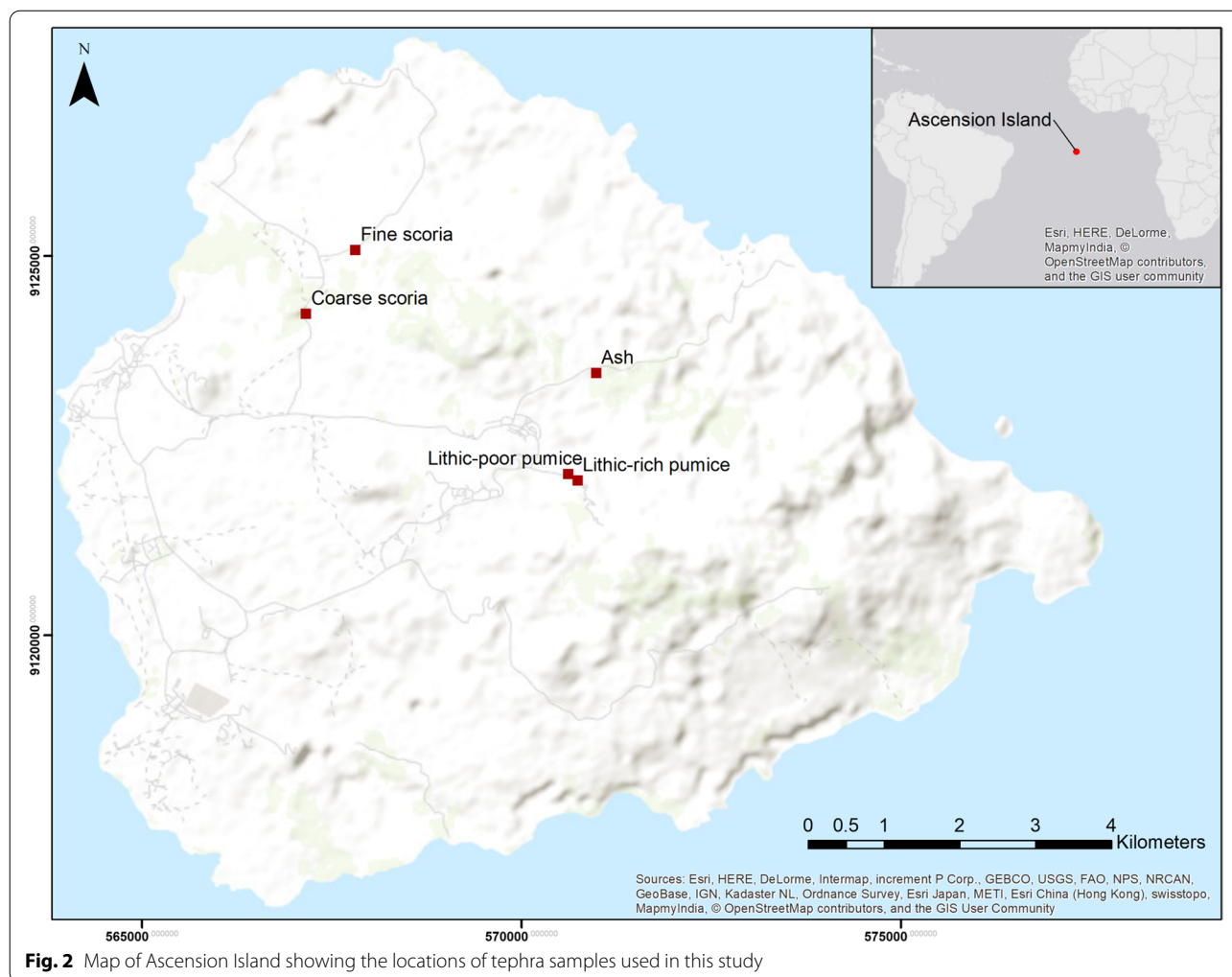
Bulk densities for dry deposits were compiled from published data for 61 eruptions at 33 volcanoes (detailed in the Appendix). These cover small to large eruptions (VEI 2–7), with mafic to silicic magma compositions, and include both proximal-medial (< 50 km from source) and distal (≥ 50 km from source) values.

Test samples were created by crushing commercially available volcanic material using a Proctor compactor to obtain a range of grain sizes. The aggregates comprised mafic 'volcanic lava filtration gravel' and silicic 'pumice

Table 1 Published grain size distribution (GSD), size and magma composition for eruptions with published GSDs ≤ 10 km from source, used in Fig. 3

Eruption	VEI	Composition	GSD distance from source (km)	Reference
Askja 1875 Unit D	5 ^a	Rhyolite	1–7	(Sparks et al. 1981)
Fogo A	5	Trachyte	~ 3–8	(Walker and Croasdale 1970; Pensa et al. 2015)
Eyjafjallajökull 2010	4	Trachyte	2–9.6	(Bonadonna et al. 2011)
Quizapu 1932	6	Dacite	2.5–7.4	(Hildreth and Drake 1992)
Agung 1963	5	Andesite	7	(Self and Rampino 2012)
Ruapehu 1996	3	Andesite	0.4	(Bonadonna et al. 2005)
Hekla 1991	3	Basaltic andesite	5	(Gudnason et al. 2017)
Calbuco 2015	4	Basaltic andesite	5–6	(Castruccio et al. 2016; Romero et al. 2016)
Etna 2002–3	3	Basalt	3.7–10	(Andronico et al. 2008)
Grimsvötn 2004	3	Basalt	5–10	(Oddsson 2007)
Kilauea Iki 1959	2	Basalt	~ 0.5–4	(Mueller et al. 2019)

^a Based on plume height of 26 km and erupted volume of 1.37 km³ for Unit D (Carey et al. 2010)



gravel’ and ‘pumice crush’ from Specialist Aggregates Ltd. Samples were then sieved to $4 \phi_g$ ($63 \mu\text{m}$) and finer grain sizes were analysed using the CAMSIZER® X2. The coarse ($\geq -4 \phi_g, \leq 16\text{mm}$) and fine ($\geq 1 \phi_g, \leq 2\text{mm}$) test GSDs were selected to be consistent with published global data and the Ascension deposits. For each test, samples were oven dried and the sample mass and volume were measured and density calculated, to ensure that test densities were consistent with our dataset of published values.

Shear box tests were used to measure the internal angle of friction of the test samples. These tests represent stress along a shear plane, as described in BS 1377-7 (British Standards Institution 1990) and use the Mohr-Coulomb equation. For dry samples (with no fluid pore pressure) the equation can be written as:

$$\tau = \sigma \tan \phi_f + c \tag{1}$$

where τ is the shear stress at failure along a plane, σ is normal stress, ϕ_f is the internal angle of friction, and c is cohesion.

For each test, the sample was loaded into the shear box and a normal force applied via a load plate. For the small shear box, this force came from calibrated weights added to a lever arm; for the large shear box, weights were added directly to the load plate for normal forces $< 1 \text{ kN}$, and via a pneumatic loading system for forces $\geq 1 \text{ kN}$. The equivalent normal stress, σ , was calculated from stress = force/area. The shear box consisted of an upper and lower section which were gradually moved relative to each other. The shear force required to move the sections was measured using a proving ring. Values were recorded throughout the test and used to calculate the equivalent shear stress, τ . Horizontal and vertical displacement in the sample were also recorded using Linear Variable Differential

Transformers (LVDT). The test finished when the shear force peaked or reached a plateau, as this represented the maximum shear stress in the sample before failure. Tests were carried out at different normal stresses (σ) and plotted against corresponding values of shear stress (τ). The internal angle of friction of the sample (ϕ_f) is the gradient of the best fit line through the data points on a σ vs τ plot (Eq. 1).

To minimise any scale effects, BS 1377-7 specifies that the largest grain size in the sample must be \leq one tenth of the specimen height in the shear box. We used small shear box tests (sample size $100 \times 100 \times 20$ mm) for samples ≤ 2 mm in diameter and large shear box tests (sample size $300 \times 300 \times 160$ mm) for samples ≤ 16 mm in diameter. We conducted tests at normal stresses of 3–35 kPa, representing deposit depths for our test samples of ~ 50 –220 cm. These depths can lead to roof failure depending on the density of the deposit (Blong 1984; Jenkins et al. 2014).

To compare ϕ_f values for the test tephra to natural samples, small shear box tests were also used to determine the internal friction angle for the Ascension ash (≤ 2 mm) samples. The sample volumes of pumice and scoria were too small to enable large shear box tests to be carried out on these materials.

Results

Near-source GSDs

Published proximal GSDs vary widely, even for eruptions with similar magma compositions (Fig. 3a-c for mafic (basalt, $\leq 52\%$ SiO₂), intermediate (basaltic andesite—andesite, 52–63% SiO₂) and silicic (dacite—rhyolite, $> 63\%$ SiO₂) eruptions detailed in Table 1). The Ascension deposits (Fig. 3d) also show coarse to fine GSDs. When all the GSDs are plotted together (Fig. 4) there is a large overlap and, for these proximal deposits, magma composition does not seem to control GSD. The coarse and fine GSDs of the test tephra (also shown on Fig. 4) were selected to be representative of both published data and the Ascension Island samples. The coarse test distribution is at the finer end of the published range of GSDs; however, a maximum grain size of 16 mm was chosen because of size constraints of the laboratory equipment, and because we are interested in the properties of the bulk deposit rather than properties of individual large clasts.

Deposit densities

Deposit densities compiled from published data reveal a range of values from ~ 400 to 1500 kg m^{-3} for all magma compositions. For individual eruptions, where

proximal/medial and distal bulk densities are reported separately, distal values are usually higher, likely indicating higher grain density and/or more efficient packing of finer grains. For some eruptions e.g. Fuego 1973 (Rose et al. 2008) textural variation in the deposits results in both low and high proximal to medial bulk densities. There is more variability in the density for low to medium silica content materials and some high silica samples have lower bulk densities. However, when the dataset is taken as a whole, there are no clear trends relating to magma composition, eruption size or distance from source (Figs. 5 and 6). Densities of the (dry) test samples are within the range of values found in the published data, as shown in Table 2.

Peak stress and internal angle of friction

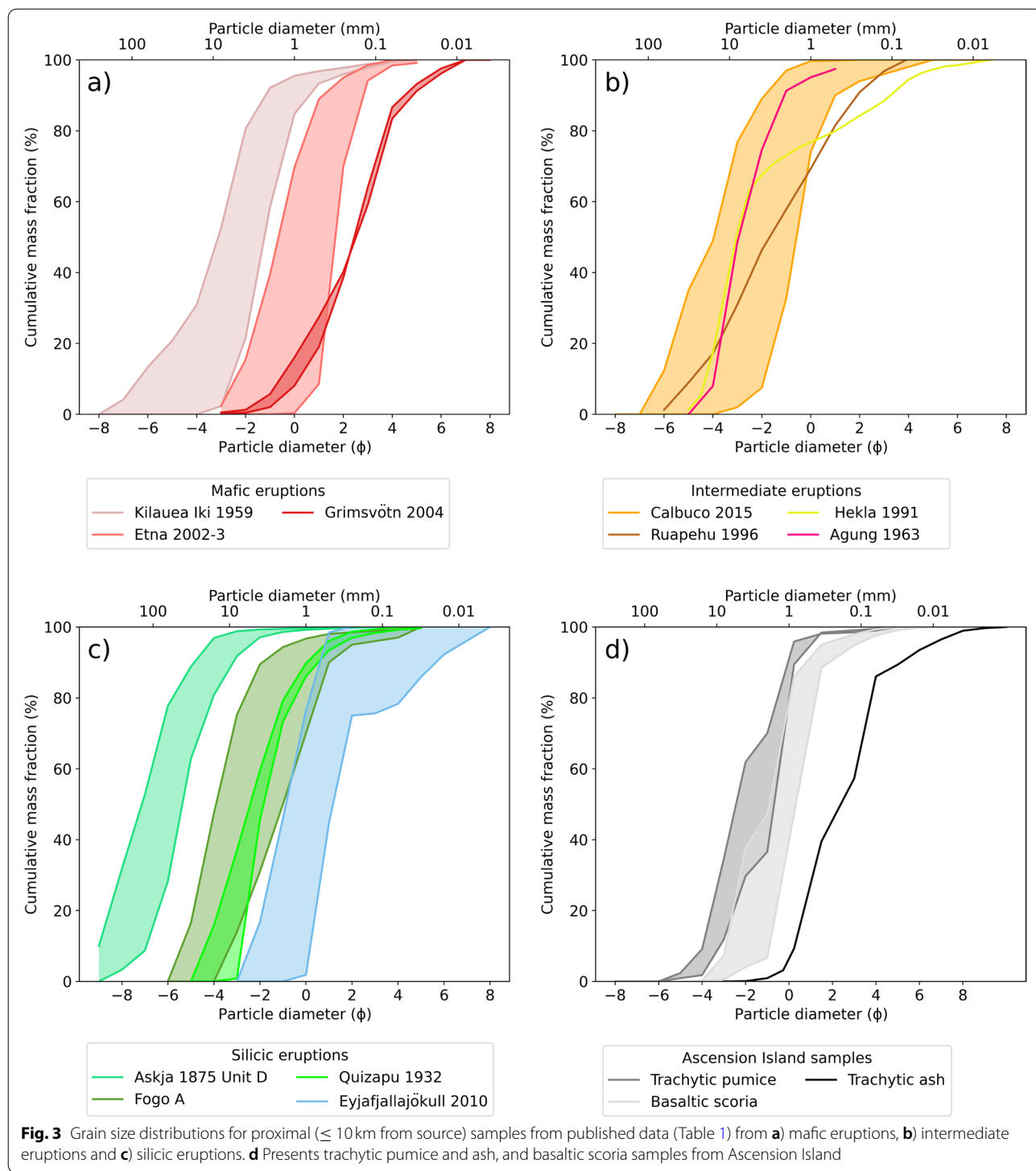
Results from the shear box tests (Figs. 7 and 8) reveal that after initial compaction, the synthetic samples dilated and shear stress reached a peak value. In comparison, the Ascension ash samples compacted throughout the tests (negative vertical displacement) and shear stress reached a plateau rather than peaking. No breaking or crushing of the grains was observed, with changes in volume achieved by rearrangement of deposit packing.

On plots of normal stress vs peak shear stress, for both pumice and scoria the coarse and fine GSDs plot on the same line (Fig. 9). The friction angles (ϕ_f), calculated using Eq. (1), are very similar for the test samples and the Ascension ash, at between 35.8 and 36.5° (Table 3). These results suggest that the internal angle of friction is independent of both tephra composition and grain size at the low normal stresses of these tests.

Discussion

Near-source grain size distribution data

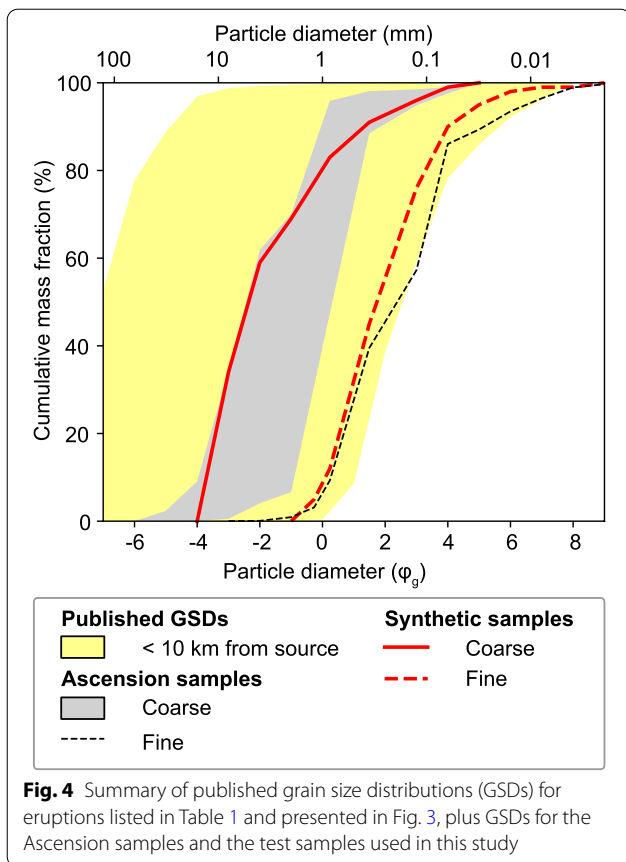
Typically GSDs of deposits become finer with increasing distance from the vent, as larger particles fall out close to source and finer particles remain in the plume (Koyaguchi and Ohno 2001a). However, the GSD of a proximal deposit depends on many factors which influence the eruption, transport and sedimentation of tephra. The magma fragmentation process influences the total grain size distribution of the erupted products (e.g. Kueppers et al. 2006; Cashman and Rust 2016), while sedimentation is affected by particle aggregation (e.g. Mueller et al. 2018; Rossi et al. 2021), plume dynamics (e.g. Scollo et al. 2017) and atmospheric conditions (e.g. Genareau et al. 2019; Poulidis et al. 2021). Our results reflect this complexity as eruptions of similar compositions show a wide range of near-source GSDs, while there is a large overlap



between samples with different compositions and from eruptions of different sizes. The Ascension samples are not fresh (with last known eruptions ≥ 500 y ago) and may have been reworked, however, the Ascension GSDs are consistent with the published data for proximal samples from 11 eruptions (Table 1).

Deposit densities

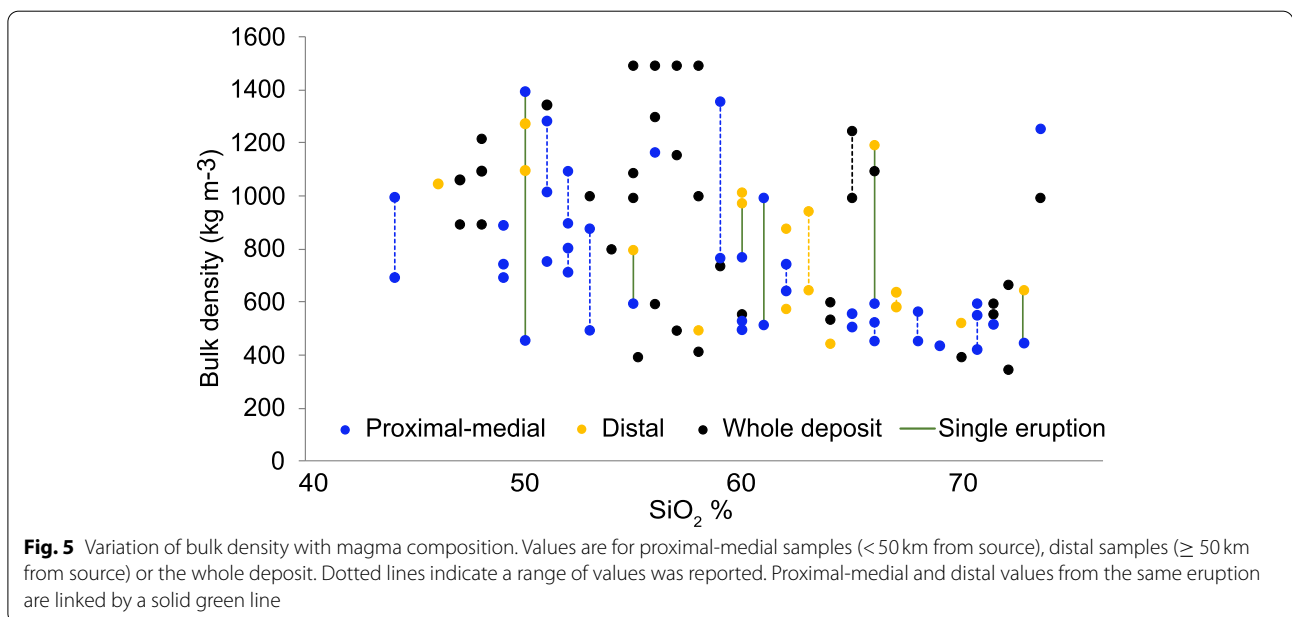
Bulk density is influenced by both the density of individual grains, degree of saturation and the deposit packing. The latter depends on grain size distribution as this affects the extent to which voids between coarser grains can be filled by finer particles. A small number of



eruptions have published data on both proximal/medial and distal bulk densities, with some having higher distal values (e.g. Thorarinsson and Sigvaldason 1972; Walker 1980; Todde et al. 2017), likely due to distal deposits having a higher crystal content or higher pumice density, as smaller particles have a relatively lower proportion of vesicles. However, this pattern is not followed for all eruptions (e.g. Thorarinsson 1954; Rose et al. 2008), particularly where the range of proximal densities is wide. Uncertainties with these data include the impact of changes over time, both short-term (compaction) and long-term (weathering), as well as the different methods used to measure deposit density. As noted in the introduction, tests in this study were only performed on dry samples, and the degree of saturation may add further uncertainty. The wide range of reported bulk densities and the lack of a clear trend relating to magma composition, eruption size or distance from source suggest these factors alone cannot reliably be used to estimate tephra loading.

Properties of synthetic samples

The GSDs and internal angles of friction of our synthetic samples matched well with the natural samples from Ascension for the grain sizes we considered ($\geq -4 \phi_g, \leq 16\text{mm}$) and the densities of the synthetic samples ($412\text{--}1532\text{kg m}^{-3}$) lie within the range of published deposit densities. These important findings provide confidence that we can use synthetic samples to test the geomechanical behaviour of tephra deposits and so avoid the difficulties and costs associated with collecting and transporting natural samples.



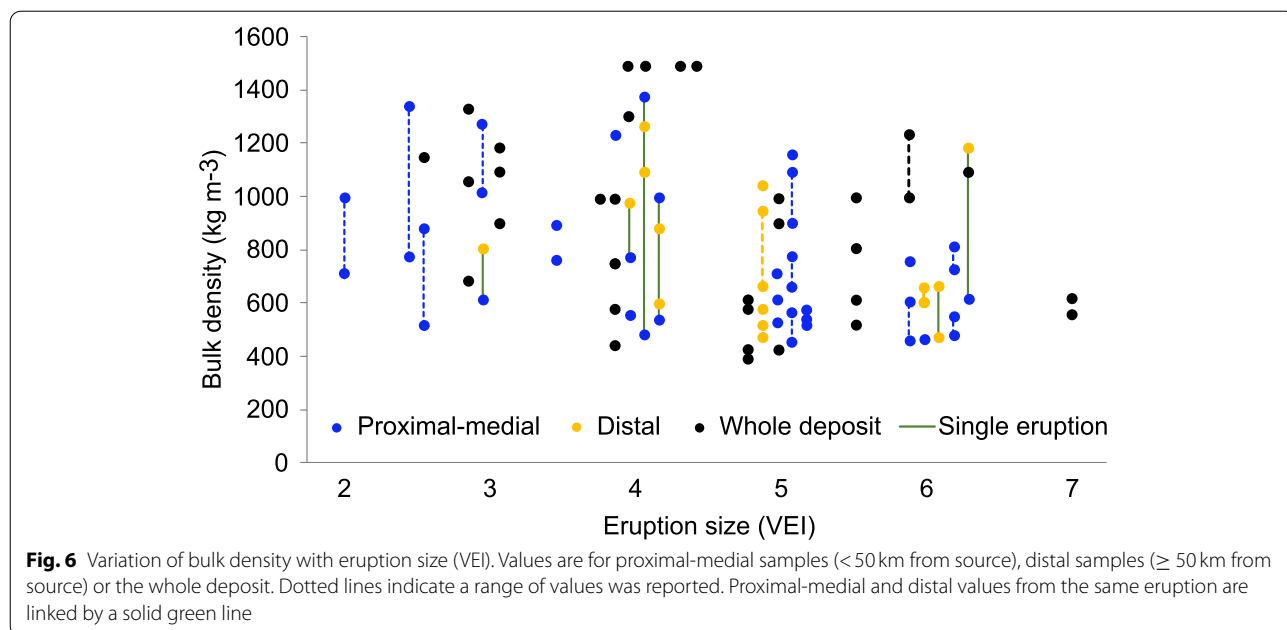


Table 2 Dry densities of test samples, and published data listed in the Appendix. Coarse and fine grain size distributions are shown in Fig. 4

Sample	Grain size distribution	Mean density (kg m ⁻³)
Synthetic pumice	Fine	602
	Coarse	412
Synthetic scoria	Fine	1532
	Coarse	1223
Ascension ash	Fine	1019
Published data	All	400–1500

Internal angle of friction

In plots of peak shear stress vs normal stress, results for coarse and fine GSDs plotted on the same line for both synthetic pumice and scoria (Fig. 9). This suggests that the friction angle is independent of grain size at the low normal stresses likely to be experienced in roof loads, where field surveys indicate that collapse can occur at ~1–10kPa (Jenkins et al. 2014). This contrasts with results at higher normal stresses (>100kPa) where the internal angle of friction has been shown to vary with grain size (e.g. Hamidi et al. 2009; Mostefa Kara et al.

2013; Alias et al. 2014). At higher normal stresses the largest grains may provide a greater barrier to movement than found in our study.

Values of the internal angle of friction were very similar for pumice and scoria (36.5° and 35.8 ° respectively) suggesting that the friction angle is also independent of magma composition and deposit density. This implies that any internal sliding of the deposit will be consistent across a range of different compositions and grain sizes, at least for the compositions and GSDs tested here. This in turn is important, as tests at one GSD could provide information about the friction angle of other GSDs. However, these results should be confirmed by laboratory sliding tests.

The peak shear stresses for the volcanic ash from Ascension Island were lower than values for the synthetic samples at similar normal stresses. The ash also compacted throughout the tests, whereas the synthetic samples mainly showed dilatatory behaviour after initial compaction. This is thought to be due to the natural sample having a higher proportion of very fine grains, which more easily reorganised and compacted into void spaces between the larger grains when stresses were applied. However, despite these differences in behaviour, the angle of friction of the Ascension ash (36.4°) was similar to the synthetic samples (36.5° and 35.8 °) and consistent with values for a range of volcanic rocks at similar normal stresses (Heap and Violay 2021). This

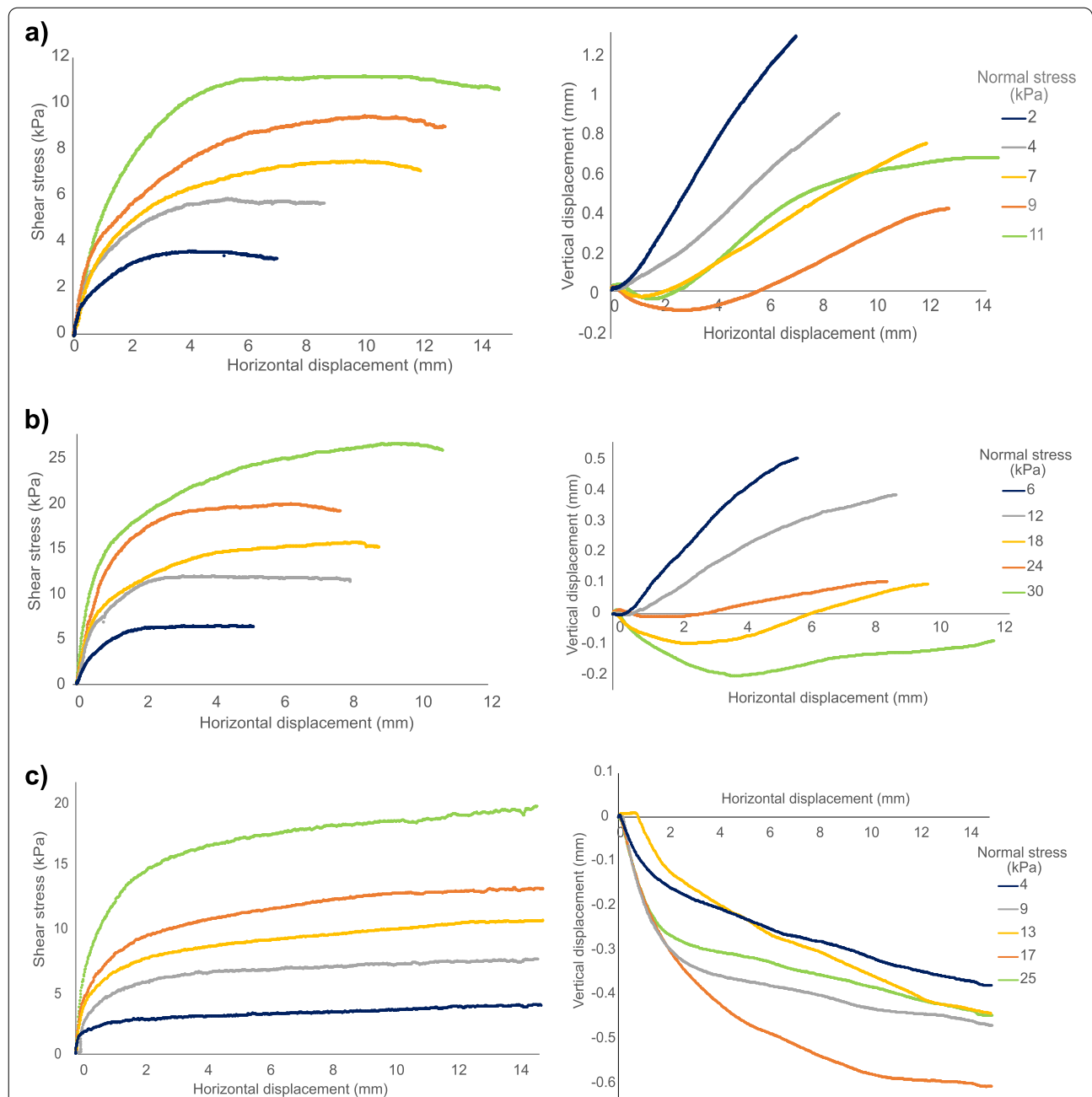


Fig. 7 Results of small shear box tests for particles ≤ 2 mm, horizontal displacement vs shear stress (left column) and horizontal vs vertical displacement (right column). **a** Synthetic pumice, **b** Synthetic scoria, **c** Ascension ash. These tests are limited by the maximum amount of travel available for the sample in the shear box. The rate of change of shear stress vs time has been examined and this shows the rate of change peaking early in the test and then subsiding to alternate between small positive and negative values oscillating around 0. Therefore, we are confident that the peak shear stress value measured is representative

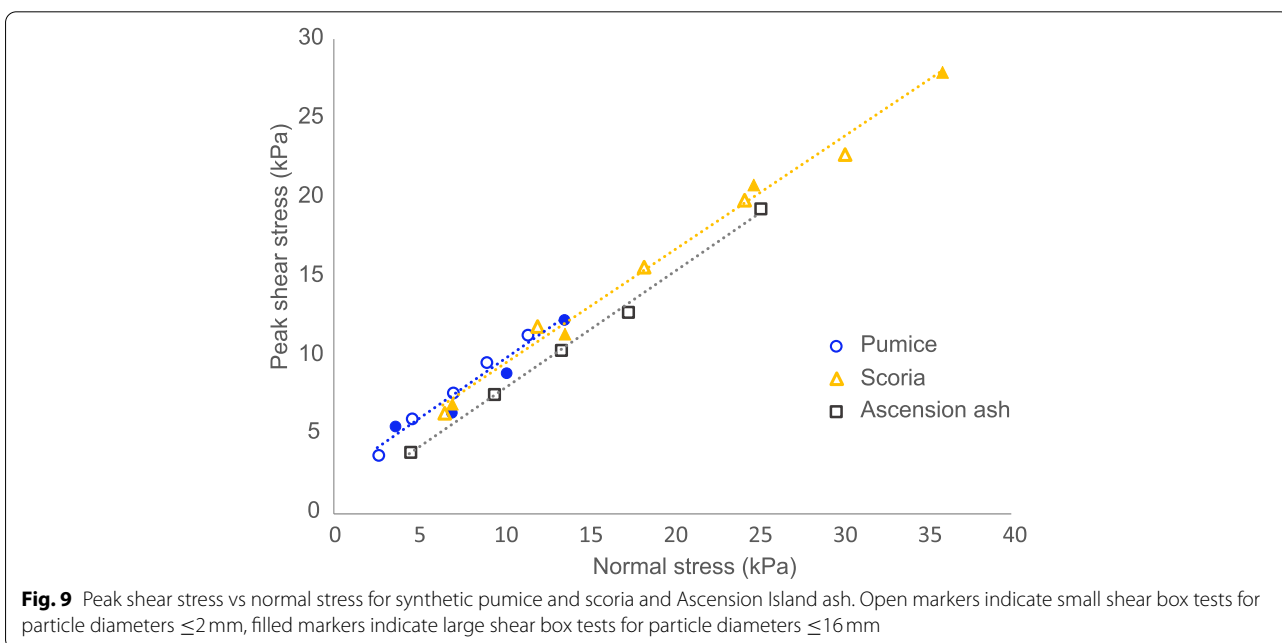
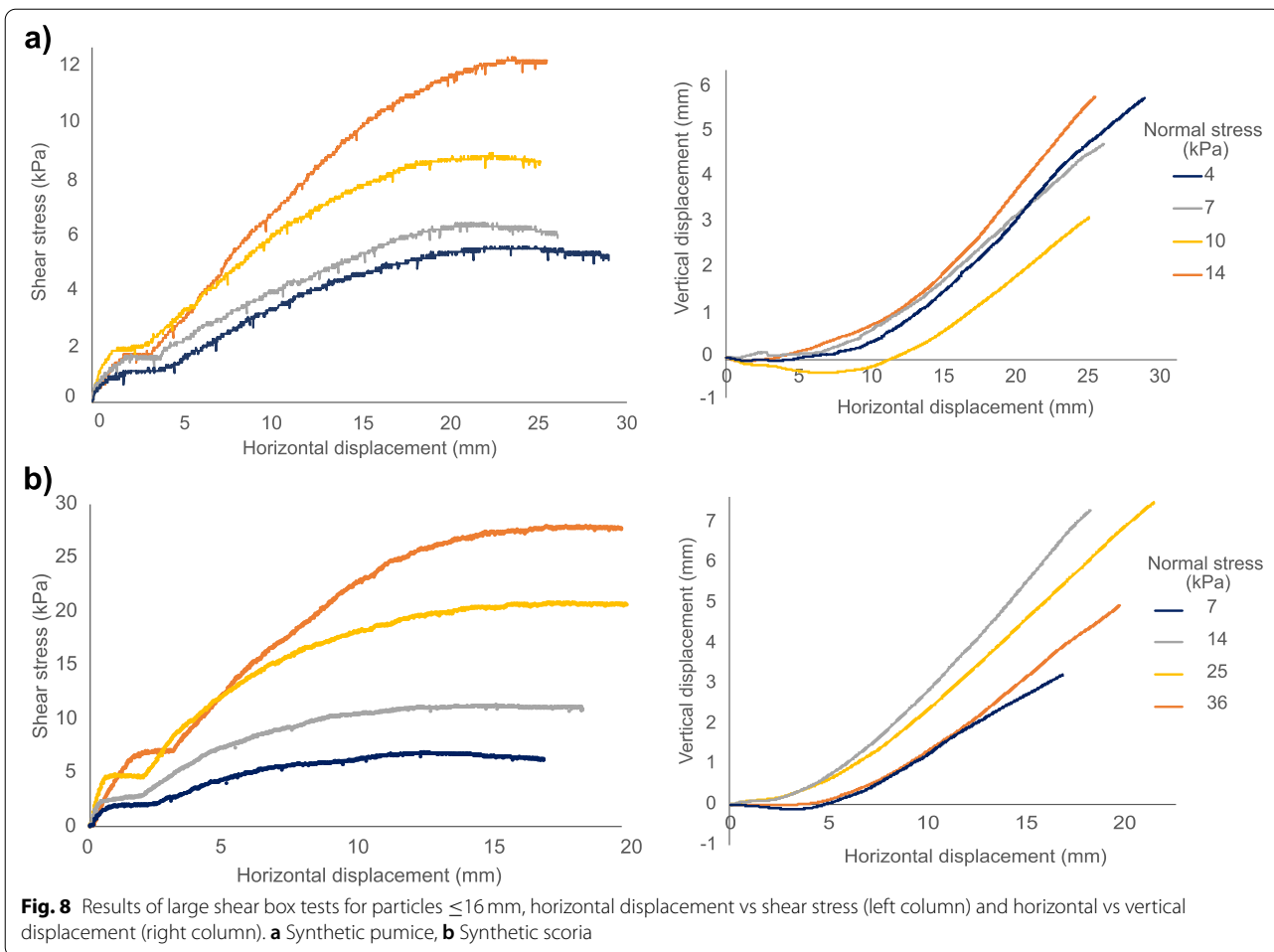


Table 3 Internal angle of friction from shear box tests for synthetic pumice and scoria and Ascension Island ash

	Friction angle (°)
Synthetic pumice	36.5
Synthetic scoria	35.8
Ascension ash	36.4

indicates that this friction angle is applicable across different tephra compositions and grain sizes, including the synthetic deposits.

The angle of repose and the internal angle of friction (ϕ_f) may not be the same, as the failure plane is constrained when ϕ_f is determined using shear box tests. However, they are both related to the frictional properties of the grains. Tests on a range of granular materials (with maximum grain size ~ 6 mm) found that the angle of repose after consolidation closely matched the internal friction angle and was independent of grain size distribution (Metcalfe 1966). This suggests that our results are relevant when considering the minimum roof pitch at which tephra will slide.

Relevance to tephra loading on roofs

The load transferred to a roof depends on the depth and density of a tephra fall deposit. Our results show that bulk density varies widely, even within a single eruption, and cannot be reliably estimated from magma composition or eruption size. Hence when assessing building vulnerability or designing new buildings to withstand tephra fall it is important to understand the range of loads likely to be experienced. This study has considered mafic and silicic deposits, with low to high bulk densities and coarse and fine GSDs and so our results are likely to be relevant when considering roof loading from future eruptions. However, our dataset should be supplemented where possible with relevant data from historic eruptions.

Limitations

This work only considered dry tephra and the addition of water would change the properties of the deposit considerably. Deposit densities have been reported to increase by 45–100% following rain (Blong 1981;

Macedonio and Costa 2012; Hayes et al. 2019; Williams et al. 2021) and further work is needed to consider how water affects bulk densities and friction angles. As our shear box tests were limited to grains $\geq -4 \phi_g$ (≤ 16 mm), we did not consider how larger particles may affect the internal angle of friction within a deposit. Aspects other than simple gravitational sliding (e.g. drifting) may also change the distribution of material on a roof and these also need further investigation. In order to understand more about tephra sliding behaviour and how this impacts the load transferred to a roof, the effect of roof properties, for example, material and pitch, must also be considered. This should be the focus of future work that will allow development of standards to account for tephra loads in building design and risk analysis.

Conclusions

We combined published data and experimental results to investigate key geomechanical properties of tephra: bulk density, grain size distribution and internal angle of friction. These properties influence roof loading and are therefore important when assessing the vulnerability of buildings to collapse.

Published tephra deposit densities and near-source grain size distributions (≤ 10 km) vary widely but there are no clear trends when considering eruptions of different compositions and sizes that can be used when assessing vulnerability.

Our laboratory experiments revealed that, at the low normal stresses likely to be experienced in roof loads (≤ 35 kPa), values of the internal angle of friction were very similar across all our tests (35.8° - 36.5°). As the friction angle influences deposit sliding behaviour, this suggests that any internal sliding of the deposit will be consistent across a range of different magma compositions, deposit densities and grain sizes.

We have shown that synthetic tephra samples, made from crushing and grading volcanic aggregates, can be used to represent natural tephra deposits in tests of geomechanical properties relevant to roof loading, regardless of eruption type or composition. This is of particular importance given the difficulty of sourcing the required volumes of natural tephra.

We considered deposits with a wide range of magma compositions, densities and grain size distributions and so we have provided an envelope of values for parameters relevant to roof loading (Tables 2 and 3), in which future eruptions are likely to sit.

Appendix

Bulk density of tephra

Data used in Figs. 5 and 6. VEI and eruption magnitude from (Croweller et al. 2012; Venzke 2013).

Eruption	VEI	Magnitude	Composition	SiO ₂ %	Bulk density (kg m ⁻³)	Reference
Agua de Pau, Fogo A 4945 BP	5	5.6	Trachyte	59–62	500 (proximal–medial)	(Walker and Croasdale 1970; Widom et al. 1992)
Agung, Bali 1963–4	5	5	Basaltic andesite	56	1170 (proximal)	(Self and King 1996; Self and Rampino 2012)
Apoyeque, Chiltepe 1.9 ka BP	6	6.3	Dacite	64–68	460–530 (proximal–medial)	(Kutterolf et al. 2011)
Apoyeque, Mateare Tephra 3–6 ka BP	5	5	Andesite–dacite	57–65	650–750 (proximal–medial)	(Kutterolf et al. 2007)
Apoyeque, Xiloa Tephra 6105 BP	5	5.3	Dacite	64–65	560 (proximal–medial)	(Kutterolf et al. 2007)
Apoyeque, Los Cedros Tephra 2–4 ka BP	5	5	Dacite	65–66	510 (proximal–medial)	(Kutterolf et al. 2007)
Apoyeque, Upper Apoyeque Pumice ~ 12.4 ka BP	5	5.6	Rhyodacite	71	430–550 (proximal–medial)	(Kutterolf et al. 2007)
Apoyeque, Lower Apoyeque Pumice ~ 17 ka BP	5	5.6	Rhyodacite	71	520 (proximal–medial)	(Kutterolf et al. 2007)
Apoyo, Lower Apoyo Tephra ~ 29 ka BP	6	6.9	Dacite	68–69	440 (proximal–medial)	(Kutterolf et al. 2007)
Apoyo, Upper Apoyo Tephra ~ 29 ka BP	6	5.8	Dacite	67–68	460–570 (proximal–medial)	(Kutterolf et al. 2007)
Askja 1875	5? 3?		Rhyolite	73	365 (mean value – unit D) 671 (mean value – unit B)	(Sparks et al. 1981; Carey et al. 2010)
Calbuco 1929	3		Andesite	59	1016 (distal, freshly fallen)	(Larsson 1936)
Calbuco 2015	4		Basaltic andesite	55	997, 1115 (mean values)	(Romero et al. 2016; Hayes et al. 2019)
Cerro Negro 1971	3		Basalt	50–53	1350 (mean value)	(Rose et al. 1973)
Chaitén 2008	4 4	4.9 4.5	Rhyolite	75 74–76	997 (distal, collected after rain) 1250 (prox–medial lithic-rich Layer β)	(Watt et al. 2009) (Alfano et al. 2011)
El Chichón 1982	5	5.1	Trachyandesite	58	500 (uncompacted); all medial–distal	(Varekamp et al. 1984)
El Chinyero 1909 (Tenerife)	2		Basanite	44	700–1000 (proximal)	(Di Roberto et al. 2016)
Cordón Caulle 2011	5	5	Rhyolite	71	560, 600 (different units, prox–distal)	(Bonadonna et al. 2015; Seropian et al. 2021)
Etna 2002–3	3		Basalt	47	1067 (mean value)	(Andronico et al. 2005; Andronico et al. 2008)
Fuego 1973	4	4.4	Basalt	47–53	460–1400 (proximal–medial) 1100–1280 (distal, mean 1140)	(Rose et al. 2008)
Grímsvötn 2004	3		Basalt	50–51	1020–1290 (proximal)	(Oddsson 2007; Jude-Eton 2013)
Gubisa Formation, Kone caldera Ethiopia	5	5.3	Rhyolite	69–72	600 (proximal)	(Rampey et al. 2014)
Hekla 1104	5	5.1	Dacite	69–70	400 (mean proximal–distal)	(Janebo et al. 2018; Geist et al. 2021)
Hekla 1300-D	4	4	Andesite	59–60	740 (mean proximal–distal)	(Janebo et al. 2018; Geist et al. 2021)
Hekla 1693	4	4.3	Andesite	59–60	560 (mean proximal–distal)	(Janebo et al. 2018; Geist et al. 2021)
Hekla 1766	4	4.3	Andesite	56–60	420 (mean proximal–distal)	(Janebo et al. 2018; Geist et al. 2021)

Eruption	VEI	Magnitude	Composition	SiO ₂ %	Bulk density (kg m ⁻³)	Reference
Hekla 1947	4	4.1	Andesite-dacite	60–63	520–1000 (proximal-medial, mean 640); 580–880 (distal, mean 800)	(Thorarinnsson 1954)
Hekla 1970	3		Basaltic andesite	55–56	600 (proximal)–800 (distal)	(Thorarinnsson and Sigvaldason 1972)
Hudson 1991	5	5.8	Trachyandesite	60–65	650–950 distal	(Scasso et al. 1994; Kratzmann et al. 2009)
Katla 1755	5?	5	Basalt	47	1050 (distal) <i>from laboratory tests</i>	(Thorarinnsson 1958)
Masaya San Antonio Tephra ~6 ka BP	6	6.3	Basalt	50–52	750 (proximal-medial)	(Kutterolf et al. 2007)
Masaya Fontana Tephra ~60 ka BP	6	6	Basaltic andesite	52	720–810 (proximal-medial)	(Kutterolf et al. 2007)
Masaya Masaya Triple Layer ~2120 BP	5	5.7	Basalt	50	700 (proximal-medial)	(Kutterolf et al. 2007)
Mount St Helens 1980	5	4.8	Dacite	63–64	450 (mean distal, 50–600 km)	(Sarna-Wojcicki et al. 1981)
Öraefajökull 1362	5	5.4	Rhyolite	69–70	560 (distal) 900 when compacted <i>from laboratory tests</i>	(Thorarinnsson 1958)
Pinatubo 1991	6	6.1	Dacite	65	1000; 1250 (different units - no change with distance from vent)	(Bernard et al. 1996; Koyaguchi and Ohno 2001b)
Quizapu 1932 freshly fallen	> 5	6	Dacite	64–70	588–644 (distal uncompact)	(Larsson 1936)
Sakurajima 1914 Taisho eruption	4	4.7	Andesite	59–62	535, 765, 980 (prox., medial, distal)	(Todde et al. 2017)
Samalas 1257 (Lombok)	7		Trachyte	64	539, 603 mean medial–distal of different units.	(Vidal et al. 2015)
Santa María, Guatemala 1902	6	6.3	Dacite	66	600 (proximal) – 1200 (distal) (average 1100)	(Williams and Self 1983; Andrews 2014)
Soufrière de Guadeloupe 1530	2–3		Andesite	55–59	1160 (mean compacted value)	(Boudon et al. 2008; Komorowski et al. 2008; Pichavant et al. 2018)
Tarawera 1886	5	5.3	Basalt	52	900 (proximal) – 1100 (medial)	(Walker et al. 1984; Rowe et al. 2021)
Taupo 232 CE	6	6.7	Rhyolite	74	450 (proximal) – 650 (distal)	(Walker 1980; Sutton et al. 1995)
Tecolote, Mexico 27 ka BP	3–4		Basalt	49	757; 894 (proximal–medial, 2 units)	(Zawacki et al. 2019)
Tungurahua 2006	2–3		Andesite	58–59	770–1360 (proximal-medial)	(Eychenne et al. 2013)
Vesuvius 1944	3		Tephrite/ phono-tephrite	45–50	1200 (mean value)	(Cioni et al. 2003; Pappalardo and Mastrolorenzo 2010)
Vesuvius 1906	3		Tephrite/ phono-tephrite	45–50	1100 (mean value)	(Cioni et al. 2003; Pappalardo and Mastrolorenzo 2010)
Vesuvius 1631	5		Phono-tephrite/ tephri-pho- nolite	52	1000 (mean value)	(Cioni et al. 2003; Pappalardo and Mastrolorenzo 2010)
Vesuvius PM1–6 (6 eruptions 512–1570)	3		Tephrite/ phono-tephrite	45–50	900 (mean value)	(Cioni et al. 2003; Pappalardo and Mastrolorenzo 2010)
Vesuvius Pollena 472	5		Phono-tephrite/ tephri-pho- nolite	46–49	900 (mean value)	(Cioni et al. 2003; Pappalardo and Mastrolorenzo 2010)
Vesuvius Pompeii White pumice 79	5–6		Phonolite	57	500 (proximal and distal)	(Cioni et al. 2003; Pappalardo and Mastrolorenzo 2010)

Eruption	VEI	Magnitude	Composition	SiO ₂ %	Bulk density (kg m ⁻³)	Reference
Vesuvius Pompeii Grey pumice 79	5–6		Tephri-phonolite	58	1000 (proximal and distal)	(Cioni et al. 2003; Pappalardo and Mastrolorenzo 2010)
Vesuvius AP5	4		Tephri-phonolite	55–60	1500 (mean value)	(Andronico and Cioni 2002; Cioni et al. 2003)
Vesuvius AP4	4		Tephri-phonolite / phonolite	52–60	1300 (mean value)	(Andronico and Cioni 2002; Cioni et al. 2003)
Vesuvius AP3 ~ 2.7 ka BP	4		Tephri-phonolite / phonolite	52–60	1500 (mean value)	(Andronico and Cioni 2002; Cioni et al. 2003)
Vesuvius AP2 ~ 3 ka BP	4–5		Tephri-phonolite / phonolite	52–60	1500 (mean value)	(Andronico and Cioni 2002; Cioni et al. 2003)
Vesuvius AP1 ~ 3.2 ka BP	4–5		Tephri-phonolite / phonolite	52–60	1500 (mean value)	(Andronico and Cioni 2002; Cioni et al. 2003)
Vesuvius Avellino White pumice ~ 3.8 ka BP	5		Phonolite	55	400 (mean value)	(Cioni et al. 2003; Pappalardo and Mastrolorenzo 2010)
Vesuvius Avellino Grey pumice ~ 3.8 ka BP	5–6		Tephri-phonolite	54	800 (proximal and distal)	(Cioni et al. 2003; Pappalardo and Mastrolorenzo 2010)
Vesuvius Mercato ~ 8 ka BP	5–6		Phonolite	52–60	600 (proximal and distal)	(Cioni et al. 2003; Pappalardo and Mastrolorenzo 2010)
Villarrica 2015	2–3		Basaltic andesite	53–55	500–880 (proximal-medial)	(Romero et al. 2018)

List of abbreviations

φ_g : Grain size (Phi scale); τ : Shear stress at failure along a plane; σ : Normal stress; φ_f : Internal angle of friction; c : Cohesion.

Acknowledgements

Many thanks to Dr. Richard Brown of Durham University for collecting samples of pumice, scoria and ash on Ascension Island and to Kirk Handley at University of Leeds for assistance with the shear box tests.

Authors' contributions

The project was devised by MT and JC and supervised by MT, JC and SC. SO undertook the data collection, laboratory work and analysis. SO wrote the manuscript with inputs from MT, JC and SC. All authors read and approved the final manuscript.

Funding

SO is supported by the Leeds-York-Hull Natural Environment Research Council (NERC) Doctoral Training Partnership (DTP) Panorama under grant NE/S007458/1. This work was in part funded by the British Geological Survey University Funding Initiative (BUFI) PhD studentship S426.

Availability of data and materials

References to published sources are listed in Table 1 and the Appendix. Shear box test data are available on request.

Declarations

Competing interests

The authors declare that they have no competing interests.

Author details

¹University of Leeds, School of Earth and Environment, Woodhouse, Leeds LS2 9JT, UK. ²British Geological Survey, The Lyell Centre, Research Avenue South, Edinburgh EH14 4AP, UK. ³University of Leeds, School of Geography, Woodhouse, Leeds LS2 9JT, UK.

Received: 2 November 2021 Accepted: 11 July 2022

Published online: 08 August 2022

References

- Alfano F, Bonadonna C, Volentik ACM, Connor CB, Watt SFL, Pyle DM, Connor LJ (2011) Tephra stratigraphy and eruptive volume of the May, 2008, Chaitén eruption, Chile. *Bull Volcanol* 73:613–630. <https://doi.org/10.1007/s00445-010-0428-x>
- Alias R, Kasa A, Taha MR (2014) Particle size effect on shear strength of granular materials in direct shear test. *World Acad Sci Eng Technol Open Sci Index* 95, Int J Civ Environ Eng 8:1144–1147
- American Society of Civil Engineers and Structural Engineering Institute 2017. ASCE/SEI 7–16: minimum design loads and associated criteria for buildings and other structures
- Andrews BJ (2014) Magmatic storage conditions, decompression rate, and incipient caldera collapse of the 1902 eruption of Santa Maria volcano, Guatemala. *J Volcanol Geotherm Res* 282:103–114. <https://doi.org/10.1016/J.JVOLGEORES.2014.06.009>
- Andronico D, Branca S, Calvari S, Burton M, Caltabiano T, Corsaro RA, Del Carlo P, Garfi G, Lodato L, Miraglia L, Murè F, Neri M, Pecora E, Pompilio M, Salerno G, Spampinato L (2005) A multi-disciplinary study of the 2002–03 Etna eruption: insights into a complex plumbing system. *Bull Volcanol* 67:314–330. <https://doi.org/10.1007/s00445-004-0372-8>
- Andronico D, Cioni R (2002) Contrasting styles of mount Vesuvius activity in the period between the Avellino and Pompeii Plinian eruptions, and some implications for assessment of future hazards. *Bull Volcanol* 64:372–391. <https://doi.org/10.1007/s00445-002-0215-4>
- Andronico D, Scollo S, Caruso S, Cristaldi A (2008) The 2002–03 Etna explosive activity: tephra dispersal and features of the deposits. *J Geophys Res*. <https://doi.org/10.1029/2007JB005126>
- Bernard A, Knittel U, Weber B, Weis D, Albrecht A, Hattori K, Klein J (1996) Petrology and geochemistry of the 1991 eruption products of mount Pinatubo. In: Newhall CG, Punongbayan R (eds) *Fire and mud: eruptions and lahars of mount Pinatubo, Philippines*. University of Washington Press, Seattle

- Blong R (2003) Building damage in Rabaul, Papua New Guinea, 1994. *Bull Volcanol* 65:43–54. <https://doi.org/10.1007/s00445-002-0238-x>
- Blong RJ (1981) Some effects of tephra falls on buildings. In: Self S, Sparks RSJ (eds) *Tephra studies*. Proc. NATO ASI "tephra studies as a tool in quaternary research", Iceland, 1980. Reidel; NATO advanced study institute studies, series C, vol 75, pp 405–420. https://doi.org/10.1007/978-94-009-8537-7_27
- Blong RJ (1984) *Volcanic hazards: a source book on the effects of eruptions*. Academic Press, Sydney
- Bonadonna C, Cioni R, Pistolesi M, Elissondo M, Baumann V (2015) Sedimentation of long-lasting wind-affected volcanic plumes: the example of the 2011 rhyolitic Cordón Caulle eruption, Chile. *Bull Volcanol*. <https://doi.org/10.1007/s00445-015-0900-8>
- Bonadonna C, Costa A (2013) Plume height, volume, and classification of explosive volcanic eruptions based on the Weibull function. *Bull Volcanol*. <https://doi.org/10.1007/s00445-013-0742-1>
- Bonadonna C, Genco R, Gouhier M, Pistolesi M, Cioni R, Alfano F, Hoskuldsson A, Ripepe M (2011) Tephra sedimentation during the 2010 Eyjafjalajökull eruption (Iceland) from deposit, radar, and satellite observations. *J Geophys Res*. <https://doi.org/10.1029/2011JB008462>
- Bonadonna C, Phillips JC, Houghton BF (2005) Modeling tephra sedimentation from a Ruapehu weak plume eruption. *J Geophys Res*. <https://doi.org/10.1029/2004JB003515>
- Boudon G, Komorowski JC, Villemant B, Semet MP (2008) A new scenario for the last magmatic eruption of La Soufrière de Guadeloupe (Lesser Antilles) in 1530 A.D.: evidence from stratigraphy radiocarbon dating and magmatic evolution of erupted products. *J Volcanol Geotherm Res* 178:474–490. <https://doi.org/10.1016/J.JVOLGEORES.2008.03.006>
- British Standards Institution (1990) BS 1377–7:1990. Methods of test for soils for civil engineering purposes. Shear strength tests (total stress). BSI, London
- British Standards Institution (2006) BS ISO 13322-2: particle size analysis. Image analysis methods. Dynamic image analysis methods. BSI, London
- British Standards Institution (2009) BS EN 1991-1-3: 2003 + A1:2015. Eurocode 1 – actions on structures. Part 1–3: general actions – snow loads. BSI, London
- Carey RJ, Houghton BF, Thordarson T (2010) Tephra dispersal and eruption dynamics of wet and dry phases of the 1875 eruption of Askja volcano, Iceland. *Bull Volcanol* 72:259–278. <https://doi.org/10.1007/s00445-009-0317-3>
- Cashman KV, Rust AC (2016) Volcanic ash: generation and spatial variations. In: Mackie S, Cashman KV, Ricketts H, Rust AC, Watson M (eds) *Volcanic ash: Hazard observation*. Elsevier, Amsterdam, pp 5–22. <https://doi.org/10.1016/B978-0-08-100405-0.00002-1>
- Cassidy M, Manga M, Cashman K, Bachmann O (2018) Controls on explosive-effusive volcanic eruption styles. *Nat Commun*. <https://doi.org/10.1038/s41467-018-05293-3>
- Castruccio A, Clavero J, Segura A, Samaniego P, Roche O, Le Pennec JL, Droguett B (2016) Eruptive parameters and dynamics of the April 2015 sub-Plinian eruptions of Calbuco volcano (southern Chile). *Bull Volcanol*. <https://doi.org/10.1007/s00445-016-1058-8>
- Cioni R, Longo A, Macedonio G, Santacroce R, Sbrana A, Sulpizio R, Andronico D (2003) Assessing pyroclastic fall hazard through field data and numerical simulations: example from Vesuvius. *J Geophys Res Solid Earth*. <https://doi.org/10.1029/2001jb000642>
- Croweller HS, Arora B, Brown SK, Cottrell E, Deline NI, Guerrero NO, Hobbs L, Kiyosugi K, Loughlin SC, Lowndes J, Nayembil M, Siebert L, Sparks RSJ, Takarada S, Venke E (2012) Global database on large magnitude explosive volcanic eruptions (LaMEVE). *J Appl Volcanol*. <https://doi.org/10.1186/2191-5040-1-4>
- Di Roberto A, Bertagnini A, Del Carlo P, Meletlidis S, Pompilio M (2016) The 1909 Chinyero eruption on Tenerife (Canary Islands): insights from historical accounts, and tephrostratigraphic and geochemical data. *Bull Volcanol*. <https://doi.org/10.1007/s00445-016-1083-7>
- Estrada N (2016) Effects of grain size distribution on the packing fraction and shear strength of frictionless disk packings. *Phys Rev E*. <https://doi.org/10.1103/PhysRevE.94.062903>
- Eychenne J, Le Pennec JL, Ramón P, Yepes H (2013) Dynamics of explosive paroxysms at open-vent andesitic systems: high-resolution mass distribution analyses of the 2006 Tungurahua fall deposit (Ecuador). *Earth Planet Sci Lett* 361:343–355. <https://doi.org/10.1016/j.epsl.2012.11.002>
- Geist D, Harpp K, Oswald P, Wallace P, Bindeman I, Christensen B (2021) Hekla revisited: fractionation of a magma body at historical timescales. *J Petrol*. <https://doi.org/10.1093/ptrology/egab001>
- Genereau K, Wallace KL, Gharghabi P, Gafford J (2019) Lightning effects on the grain size distribution of volcanic ash. *Geophys Res Lett* 46:3133–3141. <https://doi.org/10.1029/2018GL081298>
- Guðnason J, Thordarson T, Houghton BF, Larsen G (2017) The opening subplinian phase of the Hekla 1991 eruption: properties of the tephra fall deposit. *Bull Volcanol*. <https://doi.org/10.1007/s00445-017-1118-8>
- Hamidi A, Yazdanjou V, Salimi N (2009) Shear strength characteristics of sand-gravel mixtures. *Int J Geotech Eng* 3:29–38. <https://doi.org/10.3328/IJGE.2009.03.01.29-38>
- Hampton SJ, Cole JW, Wilson G, Wilson TM, Broom S (2015) Volcanic ashfall accumulation and loading on gutters and pitched roofs from laboratory empirical experiments: implications for risk assessment. *J Volcanol Geotherm Res* 304:237–252. <https://doi.org/10.1016/j.jvolgeores.2015.08.012>
- Hayes JL, Calderón R, Deline NI, Jenkins SF, Leonard GS, Mcsporrán AM, Williams GT, Wilson TM (2019) Timber-framed building damage from tephra fall and lahar: 2015 Calbuco eruption, Chile. *J Volcanol Geotherm Res* 374:142–159. <https://doi.org/10.1016/j.jvolgeores.2019.02.017>
- Heap MJ, Violay MES (2021) The mechanical behaviour and failure modes of volcanic rocks: a review. *Bull Volcanol*. <https://doi.org/10.1007/s00445-021-01447-2>
- Hildreth W, Drake RE (1992) Volcan Quizapu, Chilean Andes. *Bull Volcanol* 54:93–125. <https://doi.org/10.1007/BF00278002>
- International Standards Organization (2013) ISO 4355:2013 - bases for design of structures — determination of snow loads on roofs. ISO, Geneva
- Janebo MH, Houghton BF, Thordarson T, Bonadonna C, Carey RJ (2018) Total grain-size distribution of four Subplinian–Plinian tephra falls from Hekla volcano, Iceland: implications for sedimentation dynamics and eruption source parameters. *J Volcanol Geotherm Res* 357:25–38. <https://doi.org/10.1016/j.jvolgeores.2018.04.001>
- Jenkins SF, Spence RJS, Fonseca JFBD, Solidum RU, Wilson TM (2014) Volcanic risk assessment: quantifying physical vulnerability in the built environment. *J Volcanol Geotherm Res* 276:105–120. <https://doi.org/10.1016/j.jvolgeores.2014.03.002>
- Jude-Eton, T.C., 2013. Eruption dynamics within an emergent subglacial setting: a case study of the 2004 eruption at Grímsvötn volcano, Iceland. Ph.D. Thesis. University of Edinburgh
- Komorowski J-C, Legendre Y, Caron B, Boudon G (2008) Reconstruction and analysis of sub-plinian tephra dispersal during the 1530 A.D. Soufrière (Guadeloupe) eruption: implications for scenario definition and hazards assessment. *J Volcanol Geotherm Res* 178:491–515. <https://doi.org/10.1016/j.jvolgeores.2007.11.022>
- Koyaguchi T, Ohno M (2001a) Reconstruction of eruption column dynamics on the basis of grain size of tephra fall deposits: 1. methods. *J Geophys Res Solid Earth* 106:6499–6512. <https://doi.org/10.1029/2000jb900426>
- Koyaguchi T, Ohno M (2001b) Reconstruction of eruption column dynamics on the basis of grain size of tephra fall deposits: 2. Application to the Pinatubo 1991 eruption. *J Geophys Res Solid Earth* 106:6513–6533. <https://doi.org/10.1029/2000jb900427>
- Kratzmann DJ, Carey SN, Fero J, Scasso RA, Naranjo J-A (2009) Simulations of tephra dispersal from the 1991 explosive eruptions of Hudson volcano, Chile. *J Volcanol Geotherm Res* 190:337–352. <https://doi.org/10.1016/j.jvolgeores.2009.11.021>
- Kueppers U, Scheu B, Spieler O, Dingwell DB (2006) Fragmentation efficiency of explosive volcanic eruptions: a study of experimentally generated pyroclasts. *J Volcanol Geotherm Res* 153:125–135. <https://doi.org/10.1016/j.jvolgeores.2005.08.006>
- Kutterolf S, Freundt A, Burkert C (2011) Eruptive history and magmatic evolution of the 1.9 kyr Plinian dacitic Chiltepe tephra from Apoyeque volcano in west-central Nicaragua. *Bull Volcanol* 73:811–831. <https://doi.org/10.1007/s00445-011-0457-0>
- Kutterolf S, Freundt A, Pérez W, Wehrmann H, Schmincke HU (2007) Late Pleistocene to Holocene temporal succession and magnitudes of

- highly-explosive volcanic eruptions in west-central Nicaragua. *J Volcanol Geotherm Res* 163:55–82. <https://doi.org/10.1016/j.jvolgeores.2007.02.006>
- Landauer J, Kuhn M, Nasato DS, Foerst P, Briesen H (2020) Particle shape matters – using 3D printed particles to investigate fundamental particle and packing properties. *Powder Technol* 361:711–718. <https://doi.org/10.1016/j.powtec.2019.11.051>
- Larsson W (1936) Vulkanische Asche vom Ausbruch des chilenischen Vulkans Quizapú (1932) in Argentina gesammelt. *Bull Geol Inst Univ Upsala* 26:27–52
- Macedonio G, Costa A (2012) Brief communication: rain effect on the load of tephra deposits. *Nat Hazards Earth Syst Sci* 12:1229–1233. <https://doi.org/10.5194/nhess-12-1229-2012>
- Metcalfe JR (1966) Angle of repose and internal friction. *Int J Rock Mech Min Sci* 3:155–161. [https://doi.org/10.1016/0148-9062\(66\)90005-2](https://doi.org/10.1016/0148-9062(66)90005-2)
- Mostefa Kara E, Meghachou M, Aboubekr N (2013) Contribution of particles size ranges to sand friction. *Eng Technol Appl Sci Res* 3:497–501. <https://doi.org/10.48084/etasr.361>
- Mueller SB, Houghton BF, Swanson DA, Poret M, Fagents SA (2019) Total grain size distribution of an intense Hawaiian fountaining event: case study of the 1959 Kilauea Iki eruption. *Bull Volcanol*. <https://doi.org/10.1007/s00445-019-1304-y>
- Mueller SB, Kueppers U, Huber MS, Hess K-U, Poesges G, Ruthensteiner B, Dingwell DB (2018) Aggregation in particle rich environments: a textural study of examples from volcanic eruptions, meteorite impacts, and fluidized bed processing. *Bull Volcanol*. <https://doi.org/10.1007/s00445-018-1207-3>
- Oddsosn, B., 2007. The Grímsvötn eruption in 2004: dispersal and total mass of tephra and comparison with plume transport models. M.Sc. thesis. University of Iceland
- Pappalardo L, Mastrolorenzo G (2010) Short residence times for alkaline Vesuvius magmas in a multi-depth supply system: evidence from geochemical and textural studies. *Earth Planet Sci Lett* 296:133–143. <https://doi.org/10.1016/j.epsl.2010.05.010>
- Pensa A, Cas R, Giordano G, Porreca M, Wallenstein N (2015) Transition from steady to unsteady Plinian eruption column: the VEI 5, 4.6 ka Fogo A Plinian eruption, São Miguel, Azores. *J Volcanol Geotherm Res*. <https://doi.org/10.1016/j.jvolgeores.2015.09.012>
- Petersen GN, Björnsson H, Arason P (2012) The impact of the atmosphere on the Eyjafjallajökull 2010 eruption plume. *J Geophys Res Atmos*. <https://doi.org/10.1029/2011JD016762>
- Pichavant M, Poussineau S, Lesne P, Solaro C, Bourdier J-L (2018) Experimental parametrization of magma mixing: application to the AD 1530 eruption of La Soufrière, Guadeloupe (Lesser Antilles). *J Petrol* 59:257–282. <https://doi.org/10.1093/ptrology/egy030>
- Poulidis AP, Biass S, Bagheri G, Takemi T, Iguchi M (2021) Atmospheric vertical velocity - a crucial component in understanding proximal deposition of volcanic ash. *Earth Planet Sci Lett* 566:116980. <https://doi.org/10.1016/j.epsl.2021.116980>
- Poulidis AP, Phillips JC, Renfrew IA, Barclay J, Hogg A, Jenkins SF, Robertson R, Pyle DM (2018) Meteorological controls on local and regional volcanic ash dispersal. *Sci Rep*. <https://doi.org/10.1038/s41598-018-24651-1>
- Preece K, Barclay J, Brown RJ, Chamberlain KJ, Mark DF (2021) Explosive felsic eruptions on ocean islands: a case study from Ascension Island (South Atlantic). *J Volcanol Geotherm Res*. <https://doi.org/10.1016/j.jvolgeores.2021.107284>
- Rampey ML, Oppenheimer C, Pyle DM, Yirgu G (2014) Physical volcanology of the Gubisa formation, Kone volcanic complex, Ethiopia. *J African Earth Sci* 96:212–219. <https://doi.org/10.1016/j.jafrearsci.2014.04.009>
- Romero JE, Morgavi D, Arzilli F, Daga R, Caselli A, Reckziegel F, Viramonte J, Diaz-Alvarado J, Polacci M, Burton M, Perugini D (2016) Eruption dynamics of the 22–23 April 2015 Calbuco volcano (southern Chile): analyses of tephra fall deposits. *J Volcanol Geotherm Res* 317:15–29. <https://doi.org/10.1016/j.jvolgeores.2016.02.027>
- Romero JE, Vera F, Polacci M, Morgavi D, Arzilli F, Alam MA, Bustillos JE, Guevara A, Johnson JB, Palma JL, Burton M, Cuenca E, Keller W (2018) Tephra from the 3 March 2015 sustained column related to explosive lava fountain activity at Volcán Villarrica (Chile). *Front Earth Sci*. <https://doi.org/10.3389/feart.2018.00098>
- Rose WI, Bonis S, Stoiber RE, Keller M, Bickford T (1973) Studies of volcanic ash from two recent central American eruptions. *Bull Volcanol* 37:338–364. <https://doi.org/10.1007/BF02597633>
- Rose WI, Self S, Murrow PJ, Bonadonna C, Durant AJ, Ernst GGJ (2008) Nature and significance of small volume fall deposits at composite volcanoes: insights from the October 14, 1974 Fuego eruption, Guatemala. *Bull Volcanol* 70:1043–1067. <https://doi.org/10.1007/s00445-007-0187-5>
- Rossi E, Bagheri G, Beckett F, Bonadonna C (2021) The fate of volcanic ash: premature or delayed sedimentation? *Nat Commun* 12:1303. <https://doi.org/10.1038/s41467-021-21568-8>
- Rowe MC, Carey RJ, White JDL, Kilgour G, Hughes E, Ellis B, Rosseeel JB, Segovia A (2021) Tarawera 1886: an integrated review of volcanological and geochemical characteristics of a complex basaltic eruption. *New Zeal J Geol Geophys* 64:296–319. <https://doi.org/10.1080/00288306.2021.1914118>
- Sarna-Wojcicki AM, Shipley S, Waitt RB, Dzurisin D, Wood SH (1981) Areal distribution, thickness, mass, volume and grain size of air-fall ash from the six major eruptions of 1980. In: Lipman PW, Mullineux DR (eds) *The 1980 eruptions of Mount St. Helens*. USGS, Washington DC, pp 577–600
- Scasso RA, Corbella H, Tiberi P (1994) Sedimentological analysis of the tephra from the 12–15 August 1991 eruption of Hudson volcano. *Bull Volcanol* 56:121–132. <https://doi.org/10.1007/BF00304107>
- Scollo S, Bonadonna C, Manzella I (2017) Settling-driven gravitational instabilities associated with volcanic clouds: new insights from experimental investigations. *Bull Volcanol* 79:39. <https://doi.org/10.1007/s00445-017-1124-x>
- Self S, King AJ (1996) Petrology and sulfur and chlorine emissions of the 1963 eruption of Gunung Agung, Bali, Indonesia. *Bull Volcanol* 58:263–285. <https://doi.org/10.1007/s004450050139>
- Self S, Rampino MR (2012) The 1963–1964 eruption of Agung volcano (Bali, Indonesia). *Bull Volcanol* 74:1521–1536. <https://doi.org/10.1007/s00445-012-0615-z>
- Seropian G, Schipper CI, Harmon LJ, Smithies SL, Kennedy BM, Castro JM, Alloway BV, Forte P (2021) A century of ongoing silicic volcanism at Cordón Caulle, Chile: new constraints on the magmatic system involved in the 1921–1922, 1960 and 2011–2012 eruptions. *J Volcanol Geotherm Res*. <https://doi.org/10.1016/j.jvolgeores.2021.107406>
- Sparks RSJ, Wilson L, Sigurdsson H (1981) The pyroclastic deposits of the 1875 eruption of Askja, Iceland. *Philos Trans R Soc A Math Phys Eng Sci* 299:241–273. <https://doi.org/10.1098/rsta.1981.0023>
- Sutton AN, Blake S, Wilson CJN (1995) An outline geochemistry of rhyolite eruptives from Taupo volcanic centre, New Zealand. *J Volcanol Geotherm Res* 68:153–175. [https://doi.org/10.1016/0377-0273\(95\)00011-1](https://doi.org/10.1016/0377-0273(95)00011-1)
- Suzuki YJJ, Costa A, Koyaguchi T (2016) On the relationship between eruption intensity and volcanic plume height: insights from three-dimensional numerical simulations. *J Volcanol Geotherm Res* 326:120–126. <https://doi.org/10.1016/j.jvolgeores.2016.04.016>
- Thorarinsson S (1954) The tephra-fall from Hekla on March 29th 1947. *Erupt Hekla 1947-1948(2)*:1–68
- Thorarinsson S (1958) The Oraefajokull eruption of 1362. *Acta Naturalia Islandica* 2(2):1–99
- Thorarinsson S, Sigvaldason GE (1972) The Hekla eruption of 1970. *Bull Volcanol* 36:269–288. <https://doi.org/10.1007/BF02596870>
- Todde A, Cioni R, Pistolesi M, Geshi N, Bonadonna C (2017) The 1914 Taisho eruption of Sakurajima volcano: stratigraphy and dynamics of the largest explosive event in Japan during the twentieth century. *Bull Volcanol*. <https://doi.org/10.1007/s00445-017-1154-4>
- Varekamp JC, Luhr JF, Prestegard KL (1984) The 1982 eruptions of El Chichón volcano (Chiapas, Mexico): character of the eruptions, ash-fall deposits, and gasphase. *J Volcanol Geotherm Res* 23:39–68. [https://doi.org/10.1016/0377-0273\(84\)90056-8](https://doi.org/10.1016/0377-0273(84)90056-8)
- Venzke E (2013) *Global volcanism program: volcanoes of the world, v. 4.8.5*. <https://doi.org/10.5479/si.GVP.VOTW4-2013> Accessed 20 Jan 2021
- Vidal CM, Komorowski JC, Métrich N, Pratomio I, Kartadinata N, Prambada O, Michel A, Carazzo G, Lavigne F, Rodysill J, Fontijn K, Surono (2015) Dynamics of the major plinian eruption of Samalas in 1257 A.D. (Lombok, Indonesia). *Bull Volcanol*. <https://doi.org/10.1007/s00445-015-0960-9>
- Walker GPL (1980) The Taupo pumice: product of the most powerful known (ultraplinian) eruption? *J Volcanol Geotherm Res* 8:69–94. [https://doi.org/10.1016/0377-0273\(80\)90008-6](https://doi.org/10.1016/0377-0273(80)90008-6)
- Walker GPL, Croasdale R (1970) Two Plinian-type eruptions in the Azores. *J Geol Soc Lond* 127:17–55. <https://doi.org/10.1144/gsjgs.127.1.0017>
- Walker GPL, Self S, Wilson L (1984) Tarawera 1886, New Zealand - a basaltic plinian fissure eruption. *J Volcanol Geotherm Res* 21:61–78. [https://doi.org/10.1016/0377-0273\(84\)90016-7](https://doi.org/10.1016/0377-0273(84)90016-7)

- Watt SFL, Pyle DM, Mather TA, Martin RS, Matthews NE (2009) Fallout and distribution of volcanic ash over Argentina following the May 2008 explosive eruption of Chaitén, Chile. *J Geophys Res.* <https://doi.org/10.1029/2008JB006219>
- Widom E, Schmincke H-U, Gill JB (1992) Processes and timescales in the evolution of a chemically zoned trachyte: Fogo A, Sao Miguel, Azores. *Contrib Mineral Petrol* 111:311–328. <https://doi.org/10.1007/BF00311194>
- Williams GT, Jenkins SF, Lee DWJ, Wee SJ (2021) How rainfall influences tephra fall loading-an experimental approach. *Bull Volcanol* 83:article no: 42. <https://doi.org/10.1007/s00445-021-01465-0>
- Williams SN, Self S (1983) The October 1902 plinian eruption of Santa Maria volcano, Guatemala. *J Volcanol Geotherm Res* 16:33–56. [https://doi.org/10.1016/0377-0273\(83\)90083-5](https://doi.org/10.1016/0377-0273(83)90083-5)
- Winstanley, R., 2020. A preliminary investigation into the growth of the sisters scoria cone complex, Ascension Island. M.Sc. thesis. University of Durham
- Zawacki EE, Clarke AB, Arrowsmith JR, Bonadonna C, Lynch DJ (2019) Tecolote volcano, pinacate volcanic field (Sonora, Mexico): a case of highly explosive basaltic volcanism and shifting eruptive styles. *J Volcanol Geotherm Res* 379:23–44. <https://doi.org/10.1016/j.jvolgeores.2019.04.011>

Publisher's Note

Springer Nature remains neutral with regard to jurisdictional claims in published maps and institutional affiliations.

Ready to submit your research? Choose BMC and benefit from:

- fast, convenient online submission
- thorough peer review by experienced researchers in your field
- rapid publication on acceptance
- support for research data, including large and complex data types
- gold Open Access which fosters wider collaboration and increased citations
- maximum visibility for your research: over 100M website views per year

At BMC, research is always in progress.

Learn more biomedcentral.com/submissions

